REPORT

NANOMATERIALS

Entropy-driven stability of chiral single-walled carbon nanotubes

Yann Magnin[1]*, Hakim Amara[2], François Ducastelle[2], Annick Loiseau[2], Christophe Bichara[1]†

Single-walled carbon nanotubes are hollow cylinders that can grow centimeters long via carbon incorporation at the interface with a catalyst. They display semiconducting or metallic characteristics, depending on their helicity, which is determined during their growth. To support the quest for a selective synthesis, we develop a thermodynamic model that relates the tube-catalyst interfacial energies, temperature, and the resulting tube chirality. We show that nanotubes can grow chiral because of the configurational entropy of their nanometer-sized edge, thus explaining experimentally observed temperature evolutions of chiral distributions. Taking the chemical nature of the catalyst into account through interfacial energies, we derive structural maps and phase diagrams that will guide a rational choice of a catalyst and growth parameters toward a better selectivity.

Electronic properties of single-walled carbon nanotubes (SWNTs) depend on their chirality—i.e., the way the SWNTs are rolled along their axis— which is characterized by two indices (n, m). Controlling chirality during the tube's synthesis would enable us to avoid costly sorting and trigger the implementation of promising applications [such as the use of SWNT yarns as strong, light, and conductive wires (*1*) or the development of SWNT-based electronics (*2*)], with the ultimate goal of overcoming the limitations of silicon. Notable breakthroughs have been reported (*3*, *4*), and progress toward carbon nanotube computers (*5*, *6*) has been very rapid. However, selective synthesis still appears to be the weak link, though new studies using solid-state catalysts (*7*–*9*) have reported a chiral-specific growth of SWNTs. Detailed mechanisms underlying this selective growth are still being debated, thus underlining the need for realistic growth models explicitly including the role of the catalyst. Existing models focus on kinetics (*10*), neglecting the role of the catalyst (*11*, *12*), but fail to calculate chiral distributions in line with experiments. Atomistic computer simulations emphasize chemical accuracy (*13*, *14*) but need to be complemented with a model so as to provide a global understanding of the process. In this study, we developed a thermodynamic modeling of the interface between the tube and the catalyst to relate its properties to the resulting chiral distribution obtained during chemical vapor deposition (CVD) synthesis experiments.

Vapor-liquid-solid and vapor-solid-solid CVD processes have both been used to grow SWNTs (*8*), the latter leading to a (n, m) selectivity. Growth can proceed through tangential or perpendicular modes (*15*), and ways to control these modes have been proposed recently (*16*). For specific catalysts and growth conditions favoring the perpendicular mode, a pronounced near-armchair selectivity can be observed (*16*). In such a mode, the interface between the tube and the catalyst nanoparticle (NP) is limited to a line, and a simple model describing the thermodynamic stability of the tube-NP system can be developed. We thus considered an ensemble of configurations of a catalyst NP, possibly a metal or a carbide, in perpendicular contact with a (n, m) SWNT, as in Fig. 1. The total numbers of carbon and catalyst atoms are constant. Configurations differ by the structure of the NP-tube interface, defined by (n, m), for which we have ($n + m$) SWNT-NP bonds, with typically $10 < n + m < 50$. On the tube edge, $2m$ among the bonds are armchair, and ($n - m$) are zigzag (*17*). In a first approximation, the atomic structure of the NP is neglected, and the catalyst appears as a smooth flat surface, in a jellium-like approximation. The interface is then a simple closed loop with two kinds of species: armchair and zigzag contact atoms. Under these conditions, the total energy of the system can be separated into three terms

$$E(n, m) = E_0 + E_{\mathrm{Curv}}(n, m) + E_{\mathrm{Int}}(n, m) \quad (1)$$

where E_0 includes all terms independent of (n, m), such as the energy of the threefold coordinated carbon atoms in the tube wall and the atoms forming the NP. The surface energy of the NP and the very weak surface energy of the tube are also included in E_0, because these surfaces are kept constant. Additionally, E_{Curv} is the curvature energy, and E_{Int} is the interfacial energy. Note that this model could possibly also apply in tangential mode, if the lateral tube-catalyst interaction does not depend on (n, m).

The (n, m)-dependent energy terms concern the tube curvature and its interface with the NP. Using density functional theory (DFT) calculations, Gülseren *et al.* (*18*) evaluated the curvature energy of the isolated tube as $E_{\mathrm{Curv}} = 4\,\alpha\,D_{\mathrm{CNT}}^{-2}$, where D_{CNT} is the tube diameter and $\alpha = 2.14$ eV·Å^2 per C atom. We assume that the interfacial energy for a (n, m) tube in contact with the NP surface depends only on the number of its $2m$ armchair and (n, m) zigzag contacts

$$E_{\mathrm{Int}}^{(n,m)} = 2mE_{\mathrm{Int}}^{\mathrm{A}} + (n - m)E_{\mathrm{Int}}^{\mathrm{Z}} \quad (2)$$

where the armchair ($E_{\mathrm{Int}}^{\mathrm{A}}$) and zigzag ($E_{\mathrm{Int}}^{\mathrm{Z}}$) interfacial energies are given by $E_{\mathrm{Int}}^{\mathrm{X}} = \gamma_{\mathrm{G}}^{\mathrm{X}} + E_{\mathrm{Adh}}^{\mathrm{X}}$, with X standing for A or Z. The edge energy per dangling bond, $\gamma_{\mathrm{G}}^{\mathrm{X}}$, is positive because it is the energy cost of cutting a tube or a graphene ribbon and depends on the type of edge created. The adhesion energy of the tube in contact with the NP, $E_{\mathrm{Adh}}^{\mathrm{X}}$, is negative because energy is gained by reconnecting a cut tube to the NP. $E_{\mathrm{Int}}^{\mathrm{X}}$, the sum of these two terms, has to be positive to create a driving force for SWNT formation. DFT calculations of the edge energies of different edge configurations of a (8, 4) tube (Fig. 2) show no preferential ordering. We thus assume that all tube-catalyst interfaces with the same number of armchair and zigzag contacts have the same energy.

This leads us to introduce the edge configurational entropy as a central piece of the model. We assume that the tube is cut almost perpendicular to its axis, forming the shortest possible interface, for a given (n, m). We neglect vibrational entropy contributions, which are essentially the same for all tubes, except for radial breathing modes. Armchair twofold coordinated C atoms always come as a pair; thus, this entropy (S) that relates the number of ways of putting ($n - m$) zigzag C atoms and m pairs of armchair atoms on n sites (degeneracy) is

$$\frac{S(n, m)}{k_{\mathrm{B}}} = \ln\frac{n\,!}{m!(n - m)!} \quad (3)$$

where k_{B} is Boltzmann's constant. Interfacial energies can be evaluated using DFT calculations, described in the materials and methods. In agreement with previous studies (*17*, *19*), we find $\gamma_{\mathrm{G}}^{\mathrm{A}} = 2.06$ eV per bond and $\gamma_{\mathrm{G}}^{\mathrm{Z}} = 3.17$ eV per bond for graphene, and 1.99 and 3.12 eV

[1]Aix Marseille Université, CNRS, Centre Interdisciplinaire de Nanoscience de Marseille, Campus de Luminy, Case 913, F-13288 Marseille, France. [2]Laboratoire d'Etude des Microstructures, ONERA-CNRS, UMR104, Université Paris-Saclay, BP 72, 92322 Châtillon Cedex, France.
*Present address: MultiScale Material Science for Energy and Environment, MIT-CNRS Joint Laboratory at MIT, Cambridge, MA 02139, USA.
†Corresponding author. Email: bichara@cinam.univ-mrs.fr

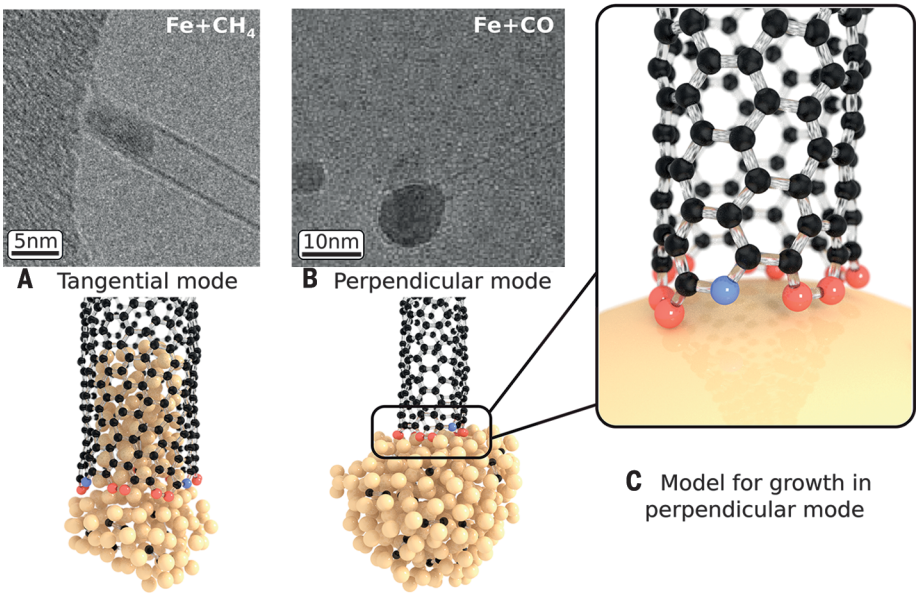

Fig. 1. From experiments to a model. (**A** and **B**) (Top) Postsynthesis transmission electron microscopy (TEM) images of a SWNT attached to the NP from which it grew at 1073 K, using either CH_4 (A) or CO (B) feedstocks, leading to a tangential or perpendicular growth mode, illustrated at the atomic scale (bottom). TEM images are reproduced from (*16*) with permission from the Royal Society of Chemistry. The experiments and our analysis of the growth modes are described in (*16*). (**C**) Sketch of the model, with a SWNT in perpendicular contact with a structureless catalyst. Armchair edge atoms are in red, zigzag ones in blue.

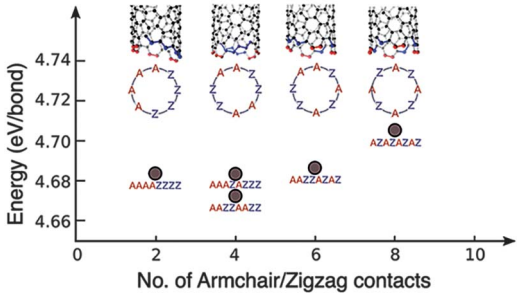

Fig. 2. Key elements of the model. (**Top**) Different ways of cutting a (8, 4) tube, leading to the formation of zigzag (blue) and armchair (red) undercoordinated atoms. For a (8, 4) tube, there are 70 different edge configurations with almost the same energy. (**Bottom**) Formation energies of all possible (8, 4) edges, from DFT calculations described in the materials and methods. The energy levels lie within 25 meV per bond and can thus be considered degenerate.

per bond, respectively, for cutting (6, 6) and (12, 0) tubes. The lower value of γ_G^A is due to the relaxation (shortening) of the C–C bonds of the armchair edge that stabilizes it. Adhesion energies of (10, 0) and (5, 5) tubes on icosahedral clusters of various metals, including Fe, Co, Ni, Cu, Pd, and Au, were calculated in (*20*, *21*). Thus, orders of magnitude for interface energies, E_{Int}^X, of armchair and zigzag terminations in contact with typical catalysts can be estimated: They lie between 0.0 and 0.5 eV per bond, with $E_{Int}^A < E_{Int}^Z$ for these metals. An example of free energy and corresponding probability distribution is plotted as a function of (n, m) in fig. S1.

Instead of focusing on a specific catalytic system, it is more relevant at this stage to study the general properties of the model that links the (n, m) indexes of a SWNT to three parameters characterizing its CVD growth conditions—namely, temperature and the interfacial energies of armchair (E_{Int}^A) and zigzag (E_{Int}^Z) tube-catalyst contacts. For each set of parameters, a free energy can be calculated, and its minimization yields the stable (n, m) value. This model displays similarities with a simple alloy model on a linear chair, but the curvature term, dominant for small diameters, and the small and discrete values of n and m prevent it from being analytically solvable, except for ground states (i.e., stable structures at zero kelvin), for which a solution is provided in the materials and methods. We thus define a three-dimensional (3D) space of stable configurations in the (T, E_{Int}^A, E_{Int}^Z) coordinates.

Setting T and, hence, the entropy contribution to zero, the ground states are readily calculated and displayed in Fig. 3A. Only armchair or zigzag tubes are found to be stable, separated by a line $E_{Int}^Z = \frac{4}{3} E_{Int}^A$. With increasing temperature, they become unstable, and a transition toward chiral tubes takes place. Figure 3B is a contour plot of the surface defined by the transition temperatures. Above this surface, for each set of (T, E_{Int}^A, E_{Int}^Z) parameters, a chiral (n, m) tube is found stable, defining "volumes" of stability for each chirality. To explore it, we can cut slices at constant temperature to obtain an isothermal stability map (Fig. 3C). In such maps, only the most stable (n, m) tube structures are shown, whereas the model yields a distribution of chiralities for each (T, E_{Int}^A, E_{Int}^Z) point. Within a (n, m) domain, this distribution is not constant, especially close to the boundaries, which are calculated by searching for points where the free energies and hence the probabilities of two competing structures are equal. As illustrated in fig. S1B, around the chirality that displays a maximal probability set to 1, neighboring chiralities have non-negligible contributions that depend on (T, E_{Int}^A, E_{Int}^Z). We can also fix either E_{Int}^A or E_{Int}^Z to obtain temperature-dependent phase diagrams, as in Fig. 4A (for $E_{Int}^A = 0.15$ eV per bond) and Fig. 4B (for $E_{Int}^Z = 0.25$ eV per bond). As an example, we can follow the temperature stability of a (6, 6) tube. Figure 4A shows a large stability range with a maximal stability temperature rising from 200 to 800 K by increasing E_{Int}^Z from 0.20 to 0.30 eV per bond, whereas the second map, orthogonal to the first one in the 3D configuration space, shows an upper temperature limit varying from 500 to 700 K, within a narrower E_{Int}^A range. Above the armchair tubes, chiral (n, $n - m$) tubes become stable starting with (n, $n - 1$) and then with increasing ($n - m$) values such as (6, 5), (7, 5), etc. Chiral tubes—i.e., tubes different from armchair or zigzag tubes—are stabilized at finite temperature by the configurational entropy of the tube edge.

An isothermal map calculated at 1000 K is plotted in Fig. 3C. Chiral tubes are spread along the $E_{Int}^Z = \frac{4}{3} E_{Int}^A$ diagonal, between armchair and zigzag ones. Small-diameter tubes are stabilized for larger values of (E_{Int}^A, E_{Int}^Z) and hence for weaker adhesion energies of the tube on the catalyst. Larger-diameter tubes are obtained for small values of (E_{Int}^A, E_{Int}^Z) because the entropy cannot counterbalance the energy cost of the interface, proportional to $n + m$. A comparison of maps at 1000 and 1400 K is provided in fig. S3. As shown in movie S1, the effect of increasing temperature is to expand and shift the stability domain of chiral tubes along and on both sides of the $E_{Int}^Z = \frac{4}{3} E_{Int}^A$ diagonal, with a larger spread on the armchair side. The stability domain of chiralities between central ($2n$, n) and near-armchair (n, $n - 1$) expands substantially at high temperature. However, the free-energy differences become smaller, leading to broader chiral distributions and thus explaining the lack of selectivity reported for tubes grown at very high temperature by electric arc or laser ablation methods (*22*).

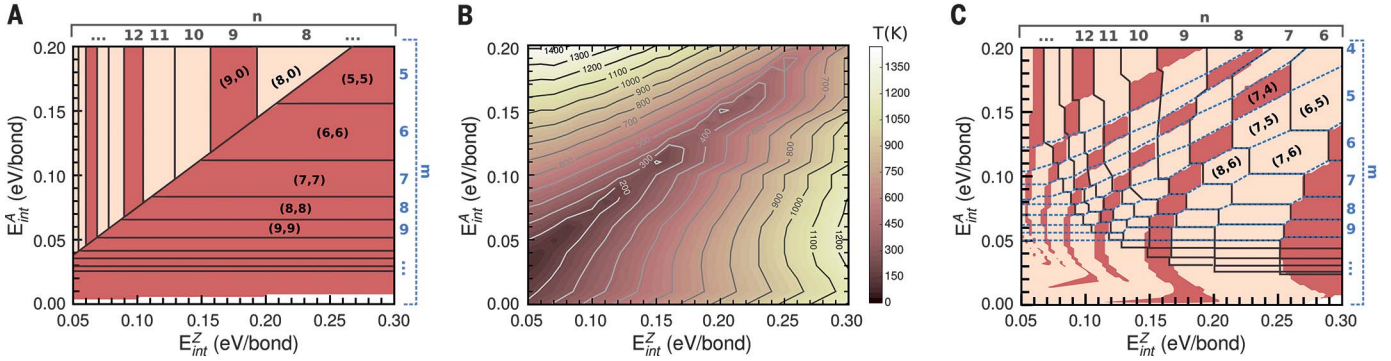

Fig. 3. Structural maps. (**A**) Map of the ground states, with armchair tubes in the lower right corner and zigzag ones in the upper left corner, separated by a line $E^{Z}_{\mathrm{Int}} = \frac{4}{3} E^{A}_{\mathrm{Int}}$. Small-diameter tubes [e.g., (5, 5) and (8, 0)] are obtained for large values of the interfacial energies E_{Int}, whereas stability domains of large-diameter tubes are narrower, with a width decaying as $\frac{1}{n(n+1)}$, and are obtained for small values of E_{Int}. (**B**) Contour plot of the highest temperatures of stability of the ground-state structures, armchair or zigzag. Chiral tubes are found only above this surface, stabilized by the configurational entropy of the tube's edge. Armchair and zigzag tubes can remain stable at high temperatures, in the bottom right and upper left corners, respectively. (**C**) Chirality map at 1000 K. Iso-n (iso-m) values are delimited by solid black (dashed blue) lines. Metallic tubes, for which $(n - m)$ is a multiple of 3, are shown in red, and semiconducting ones are flesh colored. The parameter space for armchair (metallic) and $(n, n - 1)$ and $(n, n - 2)$ (semiconducting) tubes is larger than for other chiralities.

This very simple model displays a fair agreement with literature data, as illustrated in the following examples. Figure 3B suggests a way to grow either zigzag or armchair tubes, the latter being metallic for any diameter. For both, growth kinetics is slow, because each new ring of carbon atoms has to nucleate once the previous one has been completed (*11*, *12*). To overcome this nucleation barrier, one should seek regions in the map where such tubes remain stable at high temperature. For armchair species, this corresponds to the lower right corner of the map in Fig. 3B, where the adhesion energy of armchair edges is strong and that of zigzag ones is weak, and the opposite is true for the interfacial energies. Such requirements have possibly been met in high-temperature (1473 K) CVD experiments (*23*) that also used thiophene in the feedstock. Those experiments might indicate that the presence of sulfur at the interface could modify the relative interaction strength of zigzag and armchair edges with the Fe NP.

The temperature dependence of the chiral distributions, measured by photoluminescence (*24*–*26*) or Raman and transmission electron spectroscopies (*27*) in previous studies, seems more robust. The maps presented in Fig. 4, A and B, are consistent with these experiments, showing that armchair or near-armchair chiralities [(6, 6) and (6, 5)] are grown at low temperature (873 K) and that the chiral distribution gradually shifts toward larger chiral angles [(7, 5), (7, 6), and (8, 4)...] at higher temperatures. Referring to our model, this suggests that Co- and Fe-based catalysts used in these experiments correspond to interfacial energy values around $E^{A}_{\mathrm{Int}} = 0.15$ eV per bond and $E^{Z}_{\mathrm{Int}} = 0.24$ eV per bond, as indicated by the dashed boxes in the maps. A quantitative comparison with four different sets of experimental data is provided in fig. S2, showing a slight tendency to overestimate the width of the distributions. This overestimation partly results from the fact that we use a two-parameter thermodynamic model to account for experiments that include the variability in the catalyst size and chemical composition and the growth kinetics. Our results also confirm that overlooking metallic tubes in photoluminescence experiments introduces a serious bias in the resulting chiral distribution. Further, the dependence of the quantum yield on chiral angles of semiconducting tubes may also contribute to underestimating the width of the experimental distributions.

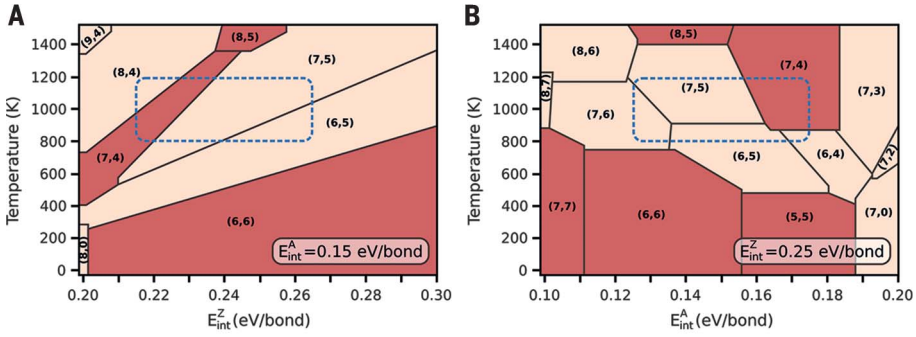

Fig. 4. Chirality phase diagrams. Phase diagrams calculated for constant values of E^{A}_{Int} (**A**) and E^{Z}_{Int} (**B**). These diagrams would be orthogonal in a 3D plot. The blue dashed boxes indicate possible parameter ranges corresponding to the analysis of growth products by He *et al*. (*26*), based on a photoluminescence assignment of tubes grown using a FeCu catalyst. (6, 5) tubes are reported stable up to 1023 K, (7, 5) and (8, 4) become dominant at 1023 K, and (7, 6) at 1073 K.

The present model thus sets a framework for understanding why a number of experiments, using metallic catalysts in perpendicular growth conditions as discussed in (*16*), report a near-armchair selectivity. For such catalysts, E^{A}_{Int} is generally lower than E^{Z}_{Int} (*20*). At low temperature, zigzag or armchair tubes are thermodynamically favored but may not always be obtained, owing to kinetic reasons. On the armchair side, our model indicates that near-armchair helicities are then favored by a temperature increase, because their stability domain is large and they are less kinetically impaired (*11*). At even higher temperatures, tube chiralities tending toward $(2n, n)$ indexes should be stabilized by their larger edge configurational entropy, but their stability domains turn out to be narrower in the present model. Taking the atomic structure of the catalyst into account in our model could rule out some neighboring structures and contribute to open up these domains.

Concerning the practical use of these maps, a first issue is to select the appropriate location for a catalyst in the $(T, E^{A}_{\mathrm{Int}}, E^{Z}_{\mathrm{Int}})$ coordinates, so as to favor the desired tube helicity. Looking at Fig. 3C, one can see that the largest and most interesting parameter ranges correspond to either metallic armchair tubes or to

(n, $n-1$) and (n, $n-2$) semiconducting tubes. A second, more difficult issue is to design a catalyst that would display appropriate $E_{\mathrm{Int}}^{\mathrm{A}}$ and $E_{\mathrm{Int}}^{\mathrm{Z}}$ values. DFT-based calculations, in the same spirit as those used in other studies (*7*, *9*, *20*, *21*, *28*), should probably be helpful. However, the evidence of the important role of the edge configurational entropy calls into question the possibility of explaining the high selectivity reported in (*7*, *9*) on the basis of a structural or symmetry matching. The intrinsic disorder at the edge could be taken into account by averaging over various atomic configurations and using molecular dynamics at finite temperature.

The present model reevaluates the role of thermodynamics in the understanding of SWNT growth mechanisms. It accounts for experimental evidence, such as the near-armchair preferential selectivity, hitherto attributed to kinetics (*11*), and the temperature-dependent trends in chiralities. It also provides a guide to design better, more selective catalysts. However, one must also consider the importance of kinetics in a global understanding of the SWNT growth process. An attempt to combine thermodynamic and kinetic aspects of the growth has been proposed in (*12*), but, overlooking the role of the edge configurational entropy, it led to unrealistic chiral distributions. Those resulting from the present thermodynamic analysis are slightly broader than the experimental distributions (fig. S2) but should be narrower if the reported chirality dependence of the growth kinetics (*11*) is taken into account. Owing to the high synthesis temperatures and the very small size of the interface, there may be SWNT growth regimes where the atomic mobility and the residence time of atoms close to the interface are large enough to achieve a local thermodynamic equilibrium.

REFERENCES AND NOTES

1. N. Behabtu *et al*., *Science* **339**, 182–186 (2013).
2. A. D. Franklin, *Nature* **498**, 443–444 (2013).
3. Q. Cao *et al*., *Science* **350**, 68–72 (2015).
4. D. Zhong *et al*., *Nat. Electron.* **1**, 40–45 (2018).
5. M. M. Shulaker *et al*., *Nature* **501**, 526–530 (2013).
6. M. M. Shulaker *et al*., *Nature* **547**, 74–78 (2017).
7. F. Yang *et al*., *Nature* **510**, 522–524 (2014).
8. M. Li *et al*., *Top. Curr. Chem.* **375**, 29 (2017).
9. S. Zhang *et al*., *Nature* **543**, 234–238 (2017).
10. A. A. Puretzky, D. B. Geohegan, S. Jesse, I. N. Ivanov, G. Eres, *Appl. Phys. A* **81**, 223–240 (2005).
11. F. Ding, A. R. Harutyunyan, B. I. Yakobson, *Proc. Natl. Acad. Sci. U.S.A.* **106**, 2506–2509 (2009).
12. V. I. Artyukhov, E. S. Penev, B. I. Yakobson, *Nat. Commun.* **5**, 4892 (2014).
13. A. J. Page, F. Ding, S. Irle, K. Morokuma, *Rep. Prog. Phys.* **78**, 036501 (2015).
14. H. Amara, C. Bichara, *Top. Curr. Chem.* **375**, 55 (2017).
15. M.-F. C. Fiawoo *et al*., *Phys. Rev. Lett.* **108**, 195503 (2012).
16. M. He *et al*., *Nanoscale* **10**, 6744–6750 (2018).
17. Y. Liu, A. Dobrinsky, B. I. Yakobson, *Phys. Rev. Lett.* **105**, 235502 (2010).
18. O. Gülseren, T. Yildirim, S. Ciraci, *Phys. Rev. B* **65**, 153405 (2002).
19. T. Wassmann, A. Seitsonen, A. M. Saitta, M. Lazzeri, F. Mauri, *Phys. Rev. Lett.* **101**, 096402 (2008).
20. F. Ding *et al*., *Nano Lett.* **8**, 463–468 (2008).
21. A. Börjesson, K. Bolton, *J. Phys. Chem. C* **114**, 18045–18050 (2010).
22. L. Henrard, A. Loiseau, C. Journet, P. Bernier, *Synth. Met.* **103**, 2533–2536 (1999).
23. R. M. Sundaram, K. K. K. Koziol, A. H. Windle, *Adv. Mater.* **23**, 5064–5068 (2011).
24. X. Li *et al*., *J. Am. Chem. Soc.* **129**, 15770–15771 (2007).
25. H. Wang *et al*., *J. Am. Chem. Soc.* **132**, 16747–16749 (2010).
26. M. He *et al*., *J. Am. Chem. Soc.* **132**, 13994–13996 (2010).
27. M. Fouquet *et al*., *Phys. Rev. B* **85**, 235411 (2012).
28. F. Silvearv, P. Larsson, S. Jones, R. Ahuja, J. A. Larsson, *J. Mater. Chem. C* **3**, 3422–3427 (2015).

ACKNOWLEDGMENTS

Funding: Support from the French research funding agency (ANR) under grant 13-BS10-0015-01 (SYNAPSE) is gratefully acknowledged. C.B. thanks P. Müller for stimulating discussions. **Author contributions:** C.B. designed the project; Y.M., H.A., F.D., and C.B. developed the model; and all authors contributed to the data analysis and manuscript preparation. **Competing interests:** The authors declare no competing interests. **Data and materials availability:** All data are available in the main text or the supplementary materials.

SUPPLEMENTARY MATERIALS

www.sciencemag.org/content/362/6411/212/suppl/DC1
Materials and Methods
Figs. S1 to S3
References (*29*–*35*)
Movie S1
Data S1 and S2

21 March 2018; accepted 8 August 2018
10.1126/science.aat6228

Entropy-driven stability of chiral single-walled carbon nanotubes

Yann Magnin, Hakim Amara, François Ducastelle, Annick Loiseau and Christophe Bichara

Science **362** (6411), 212-215.
DOI: 10.1126/science.aat6228

The twisted carbon nanotube story

Despite progress in growing single-walled carbon nanotubes of specific size and chirality, the factors that control their growth are still not fully known. Magnin *et al.* developed a thermodynamic model for the growth of single-walled carbon nanotubes. The model explains the origin of nanotube chirality in terms of the configurational entropy of the nanotube edge. The model should be useful in helping to guide nanotube growth parameters to enhance selectivity.

Science, this issue p. 212